Molecular Cancer Therapeutics

Reversal of Chemoresistance in Ovarian Cancer by Co-Delivery of a P-Glycoprotein Inhibitor and Paclitaxel in a Liposomal Platform

Yilin Zhang[1], Shravan Kumar Sriraman[2], Hilary A. Kenny[1], Ed Luther[2], Vladimir Torchilin[2], and Ernst Lengyel[1]

Abstract

The overexpression of permeability-glycoprotein (P-gp), an ABC transporter involved in the cellular exclusion of chemotherapeutic drugs, is a major factor in paclitaxel-resistant ovarian cancer. However, in clinical trials, co-administration of P-gp inhibitors and anticancer drugs has not resulted in the efficient reversal of drug resistance. To improve administration, we encapsulated the third-generation P-gp inhibitor tariquidar (XR-9576, XR), alone or in combination with paclitaxel (PCT) in liposomes (LP). After optimization, the liposomes demonstrated favorable physicochemical properties and the ability to reverse chemoresistance in experiments using chemosensitive/chemoresistant ovarian cancer cell line pairs. Analyzing publicly available datasets, we found that overexpression of *P-gp* in ovarian cancer is associated with a shorter progression-free and overall survival. *In vitro*, LP(XR) significantly increased the cellular retention of rhodamine 123, a P-gp substrate. LP(XR,PCT) synergistically inhibited cell viability, blocked proliferation, and caused G_2–M arrest in paclitaxel-resistant SKOV3-TR and HeyA8-MDR cell lines overexpressing P-gp. Holographic imaging cytometry revealed that LP(XR,PCT) treatment of SKOV3-TR cells induced almost complete mitotic arrest, whereas laser scanning cytometry showed that the treatment induced apoptosis. In proof-of-concept preclinical studies, LP(XR,PCT), when compared with LP(PCT), significantly reduced tumor weight (43.2% vs. 16.9%, $P = 0.0007$) and number of metastases (44.4% vs. 2.8%, $P = 0.012$) in mice bearing orthotopic HeyA8-MDR ovarian tumors. In the xenografts, LP(XR,PCT) efficiently induced apoptosis and impaired proliferation. Our findings suggest that co-delivery of a P-gp inhibitor and paclitaxel using a liposomal platform can sensitize paclitaxel-resistant ovarian cancer cells to paclitaxel. LP(XR,PCT) should be considered for clinical testing in patients with P-gp–overexpressing tumors. *Mol Cancer Ther; 15(10); 2282–93. ©2016 AACR.*

Introduction

Ovarian cancer is the deadliest gynecologic malignancy in developed countries. It has a 5-year survival rate of approximately 40% and accounts for 6% of all cancer-related deaths in women in the United States (1, 2). The current standard of care includes debulking surgery and subsequent adjuvant chemotherapy with paclitaxel and carboplatin. Although combination chemotherapy clearly prolongs the lives of patients with ovarian cancer, the disease recurs in 80% of cases because the tumor cells develop drug resistance (3, 4). A modest increase in survival has been achieved with intraperitoneal chemotherapy, but the complications associated with peritoneal catheters currently impede their widespread clinical adoption (5).

Since the discovery of multidrug resistance (MDR) about 4 decades ago (6), tremendous efforts have been made to elucidate its mechanisms. So far, three major mechanisms of MDR have been identified and explored: (i) plasma membrane ATP-binding cassette (ABC) transporters extrude drugs, preventing intracellular accumulation (4, 7, 8); (ii) transmembrane importers regulate the entry of water-soluble drugs (9, 10); and (iii) a constellation of contributing factors such as epigenetic modifications (11, 12), miRNAs (13, 14), and elements of the tumor microenvironment, which work together to induce drug resistance (15, 16).

Permeability-glycoprotein (P-gp, MDR1, ABCB1; refs. 17, 18) and multidrug resistance associated-protein 1 (MRP1, ABCA1; ref. 4) are 2 important ABC transporters associated with drug resistance in ovarian cancer. P-gp was the first ABC member found to confer chemoresistance and is still seen as one of the most promising targets for the reversal of chemoresistance (17). The overexpression of P-gp is associated with reduced progression-free and overall survival in several cancer types, including ovarian cancer (19–22), most probably because it contributes to the cellular exclusion of a broad spectrum of chemotherapeutic drugs, including taxanes, doxorubicin, and vinca alkaloids (8). The energy-dependent efflux of the chemotherapeutic drugs out of the cancer cell reduces the intracellular

[1]Department of Obstetrics and Gynecology/Section of Gynecologic Oncology, University of Chicago, Chicago, Illinois. [2]Center for Pharmaceutical Biotechnology and Nanomedicine, Northeastern University, Boston, Massachusetts.

Note: Supplementary data for this article are available at Molecular Cancer Therapeutics Online (http://mct.aacrjournals.org/).

Y. Zhang and S.K. Sriraman contributed equally to this article.

Corresponding Author: Ernst Lengyel, Department of Obstetrics and Gynecology, University of Chicago, 5841 South Maryland Avenue, Chicago, IL 60637. Phone: 773-834-0563; Fax: 773-702-5161; E-mail: elengyel@uchicago.edu

doi: 10.1158/1535-7163.MCT-15-0986

accumulation of otherwise effective therapies, requiring a higher dose to achieve an anticancer effect. Therefore, inhibiting P-gp to increase the length of time a drug remains inside the cell represents a reasonable strategy for the reversal of chemoresistance. Downregulating P-gp expression with RNA interference or blocking P-gp activity with inhibitors has been shown to sensitize chemoresistant cancer cells to chemotherapy in various cancers (23). Three generations of P-gp inhibitors have been identified. The first 2 generations of P-gp modulators, such as cyclosporine A and verapamil, function by competitively binding substrates at the transmembrane domain; but, although they successfully compete for substrate binding, they display low specificity and significant side effects (7). Tariquidar (XR9576), a third-generation inhibitor (24), is a noncompetitive inhibitor of P-gp which impedes drug efflux by blocking the transition of P-gp to an open conformation (25). However, clinical trials with tariquidar had to be terminated early because of the ability of inhibitor to block normal physiologic functions of P-gp. P-gp, when highly expressed, acts to maintain the blood–brain barrier and exclude toxins from normal tissues, notably those of the intestines, kidney, and spleen (as reviewed in ref. 26).

To limit the effects of tariquidar on normal tissue, as well as overcome its unfavorable pharmacokinetic properties, such as low water solubility and short serum half-life (4, 10), an effective systemic delivery approach with improved pharmacokinetic profiling and tumor targetability is necessary. Encapsulating tariquidar and paclitaxel in nanoparticles represents one such strategy, as nanoparticles are known to passively accumulate at tumor sites due to enhanced permeability and retention (EPR) caused by leaky malignant tumor vasculature (27). In addition, nanoparticles confer more favorable pharmacokinetic profiles to the encapsulated substances (28). Indeed, poly (D,L-lactide-co-glycolide) (PLGA)-formulated nanoparticles delivering paclitaxel and tariquidar were reported to efficiently reduce subcutaneous mammary tumor growth in a paclitaxel-resistant mouse model (29).

In view of the important role of P-gp in ovarian cancer chemotherapy resistance in general and paclitaxel resistance specifically and given that tariquidar has been established as an efficient P-gp inhibitor, our goal was to determine whether tariquidar/paclitaxel nanoparticles are a viable strategy that should be further developed for treatment of paclitaxel-resistant ovarian cancer. We hypothesized that co-administration of the P-gp inhibitor and paclitaxel using a liposomal platform could achieve synergistic effects, increasing the retention of paclitaxel in chemotherapy-resistant ovarian cancer, thereby significantly reducing the effective dose of paclitaxel required to kill tumor cells. Using paclitaxel-sensitive/resistant cell line pairs, we report here that liposomes encapsulating both tariquidar and paclitaxel increase the cytotoxicity of paclitaxel and effectively inhibit chemoresistant ovarian cancer tumor growth in a preclinical model.

Materials and Methods

Reagents

Egg phosphatidylcholine (ePC), cholesterol, and a handheld mini extruder were purchased from Avanti Polar Lipids. 1,2-Distearoyl-*sn*-glycero-3-phosphoethanolamine-*N*-[methoxy (polyethylene glycol)-2000] (DSPE-PEG_{2000}) and 1,2-dioleoyl-3-trimethylammonium-propane (DOTAP) were purchased from Corden Pharma International. Tariquidar and paclitaxel were obtained from Medkoo Biosciences and LC Labs, respectively. Rhodamine 123 was purchased from Sigma-Aldrich. CellTiter-Blue Cell Viability Assay was obtained from Promega. The X-Bridge C18 column (4.6 × 250 mm^2, 5 μm id) was from Waters. Hoechst 33342, Yo-Pro, and propidium iodide (PI) were purchased from Life Technologies. Fluorescein isothiocyanate (FITC)-labeled P-gp (UIC-2), phycoerythrin (PE)-labeled MRP-1 (QCRL-1), β-tubulin (G-8), and goat anti-mouse IgG-FITC antibodies were purchased from Santa Cruz Biotechnology. CDC25C (5H9), p21 (12D1), GAPDH (14C10), phosphorylated CDC2 (Tyr15, 10A11), and total CDC2 antibodies were obtained from Cell Signaling Technology, whereas cyclin B1 (S126) and P-gp antibodies were purchased from Abgent. Cleaved caspase-3 (Asp175) antibody was from Cell Signaling Technology. Ki-67 antibody (SP6) and high-performance liquid chromatography (HPLC)-grade acetonitrile were from Thermo Fisher Scientific.

Cell culture

SKOV3ip1 and HeyA8 cells were provided by Dr. Gordon Mills (MD Anderson Cancer Center, Houston, TX). HeyA8-MDR was a gift from Dr. Anil Sood (MD Anderson Cancer Center; ref. 30). SKOV3-Taxol–resistant cells (TR) were provided by Dr. Zhenfeng Duan (MGH, Boston, MA; ref. 31). Tyk-nu cells were provided by Dr. Kenjiro Sawada (Osaka University, Osaka, Japan; ref. 32). The Tyk-nu carboplatin-resistant (R) cell line (33) was purchased from JCRB cell bank. Tyk-nu and Tyn-nu-R cells were cultured in Eagle minimum essential medium with 15% FBS, 1% penicillin/streptomycin, and 1% L-glutamine (34). All other human ovarian cancer cell lines were maintained in DMEM with 10% FBS and 1% penicillin/streptomycin solution at 37°C with 5% CO_2. All cell lines were authenticated using the commercial service, CellCheck (IDEXX Bioresearch). Samples were confirmed to be of human origin and no mammalian interspecies contamination was detected. The alleles for 9 short tandem repeat (STR) markers were determined and the results were compared with the profiles from DSMZ, ATCC, JCRB, and RIKEN STR databases.

Preparation of liposomes

Liposomes were synthesized by the thin-film hydration method (35). Briefly, a lipid film of ePC, cholesterol, and DOTAP mixed at a mole ratio of 64%:30%:6% with tariquidar and paclitaxel (equimolar amounts at a 1% w/w ratio to the total lipid) was prepared by removal of organic solvents using rotary evaporation followed by freeze-drying overnight. The lipid film was hydrated with PBS (pH = 7.4) to a 5 mg/mL lipid concentration and then extruded through 200-nm polycarbonate membranes. The nonencapsulated, insoluble, hydrophobic drug was then removed by syringe filtration (0.22-μm filter). A film of the PEG_{2000}-DSPE at a mole ratio of 2% (to the total lipid in the liposome) was hydrated with the liposomal solutions and was constantly stirred at 37°C overnight. For *in vivo* studies, the lipid film was rehydrated to a 40 mg/mL lipid concentration.

Physicochemical characterization of liposomes

Particle size and zeta potential were measured using an N4 Coulter Particle Size Analyzer and Zeta*plus* (Brookhaven Instruments Corporation), respectively. The particle size and surface morphology was further confirmed with a uranyl acetate stain

using transmission electron microscopy (TEM). The liposomal drug concentrations were determined by reverse phase HPLC using an X-bridge C18 column on a Hitachi Elite LaChrom HPLC system. A mixture of 10 mmol/L ammonium acetate buffer (pH = 4; 40%) and acetonitrile (60%) was used as the mobile phase with a 1-mL/minute flow rate. The tariquidar had a retention time of about 3.2 minutes whereas paclitaxel had a retention time of about 5.3 minutes. Detection of both drugs was carried out using a UV detector (228 nm). Liposomal drug concentrations were calculated by comparison against a standard curve of each drug (0–20 μg/mL). The characterization of drug-loaded liposomes is described in Supplementary Table S1.

Kaplan–Meier survival analysis

We performed Kaplan–Meier survival analyses on the basis of P-glycoprotein (*P-gp*/*ABCB1* gene) expression in patients with ovarian cancer using the Gene Expression Omnibus (GEO) and The Cancer Genome Atlas (TCGA) database. The cut-off level of expression dividing the high or low groups was determined by an algorithm of the Kaplan–Meier plotter (36, 37). Accession numbers for gene expression datasets were: GSE-14764, -15622,-18520, -19829, -23554, -26193, -26712, -27651, -30161, -3149, -51373, -9891, and TCGA. The expression range of the P-gp probe (209994_s_at) was 2 to 1,918. Progression-free survival (PFS) was calculated for each dataset ($n > 1{,}000$; follow-up for 15 years) with the cut-off level of 43. Overall survival (OS) rate was assessed for each dataset ($n = 1{,}339$; follow-up for 20 years) with a cutoff level of 64. The expression range of the *MRP1* probe (205887_x_at) was 11 to 1,815, and the expression range of the *MRP3* probe (208161_s_at) was 3 to 5,163. PFS was calculated for each dataset ($n = 1{,}056$; follow-up for 15 years) with the cut-off level of 393 (*MRP1*) and 101 (*MRP3*).

Flow cytometry analysis of P-gp and MRP1 expression

HeyA8, HeyA8-MDR, SKOV3, SKOV3-TR, Tyk-nu, and Tyk-nu-R cells were harvested using nonenzymatic CellStripper solution (Corning Inc.) to preserve membrane integrity. After washing, the cells (5×10^5) were stained with 10 μL of either FITC-labeled anti–P-gp antibody or PE-labeled anti-MRP1 antibody on ice for 30 minutes. After spinning down, cells were resuspended in HBSS with 1% FBS and expression was analyzed by an LSR II Fortessa cell analyzer (BD Biosciences; ref. 38). The data were processed by FlowJo software (Tree Star Inc).

Rhodamine 123 exclusion assay

HeyA8/HeyA8-MDR and SKOV3ip1/SKOV3-TR cells were treated with free tariquidar (140 nmol/L, XR) or liposomal tariquidar (14 nmol/L, XR) for 48 hours. The cells were then trypsinized, washed, and stained with 1 μmol/L of rhodamine 123, a fluorescent substrate of P-gp, in an incubator for 30 minutes (35). The cells were spun down, resuspended in ice-cold HBSS with 1% FBS, and analyzed by the LSR II Fortessa cell analyzer. The data were processed by FlowJo software.

Laser scanning cytometry

To measure apoptosis, SKOV3-TR cells (3×10^3) were seeded on black 96-well plates 24 hours prior to the experiment. Liposomes were sterile filtered through 0.2-μm filters and incubated with the cells for 24 hours and washed off. After a further 24 hours, 3 fluorescent dyes [Hoechst 33342 (5 μg/mL), Yo-Pro (0.063 μg/mL), and PI (1 μg/mL)] were added to stain live cell nuclei, cells in early apoptosis (slight membrane permeability), and late apoptosis/necrosis, respectively. After incubation at 37°C for 30 minutes, the cells were analyzed *in situ* using the iCyte laser scanning cytometer (CompuCyte Corp.; refs. 39, 40). Excitation/emission wavelengths used were 405/440 nm with a 30-nm bandwidth for Hoechst, 488/515 nm with a 30-nm bandwidth for Yo-Pro, and 488/635 nm for PI. All data analyses were carried out using the iCyte Software (Version 3.4). Alternatively, DNA content distributions were measured by PI staining. Upon treatment with liposomes (50 nmol/L paclitaxel; 40 nmol/L XR) for 18 hours, the cells were permeabilized by 70% ethanol overnight, stained with PI/RNase buffer (BD Biosciences), and detected by an LSR II Fortessa cell analyzer. The cell-cycle distributions were further processed by FlowJo software (38).

In vitro cytotoxicity

Cells (3×10^3) were seeded in each well of a 96-well plate 24 hours prior to the experiments. Liposomes (50 or 100 nmol/L paclitaxel) were incubated with the cells for 7 days. Cell viability was then measured using a CellTiter-Blue Cell Viability Assay kit. The living cells are able to convert resazurin, a redox dye, to fluorescent resorufin, whereas the dying or dead cells could not. The fluorescent signals were detected via a Synergy HT plate reader (Bio-Tek) with an excitation wavelength of 530 nm and emission of 590 nm.

Colony formation assays

Cell proliferation upon liposome treatment was examined by two types of colony formation assays: monolayer and soft agar (41). For monolayer colony formation, cells were seeded onto 24-well plates and treated with free or liposomal drugs (100 nmol/L paclitaxel; 90 nmol/L XR) for 7 days before fixation, crystal violet staining and imaging (G-box, Syngene). For soft agar colony formation, the cells mixed with 0.4% agar/medium were seeded onto 0.8% agar/medium support in 6-well plates and treated with the liposomes (100 nmol/L paclitaxel) for 40 days with the media changed every week. Cells were fixed, stained with crystal violet, and imaged with the G-Box bioimaging system.

Scratch assay

HeyA8-MDR/HeyA8, SKOV3-TR/SKOV3-TR (3×10^3) cells were seeded in a 96-well plate. Scratches were generated using a 96-pin wound maker (Essen BioScience) and cells were treated with free tariquidar (XR), paclitaxel, LP(XR), LP(PCT), or LP(XR, PCT) (50 nmol/L paclitaxel; 40 nmol/L XR) or not treated. The cells were imaged in real-time every 2 hours using an IncuCyte system (Essen BioScience) with phase-contrast microscopy at a 10× magnification (42, 43). Changes in confluence of the wound/scratch were quantified by Zoom software (Essen BioScience).

Holographic imaging cytometry

SKOV3-TR (2×10^5) cells were seeded in T-25 flasks for 48 hours prior to the experiment. The cells were incubated with liposomes (100 nmol/L paclitaxel) and imaged every 5 minutes for 48 hours using the holographic imaging cytometer HoloMonitor M4 (Phase Holographic Imaging AB), which employs a low-power 635 nm red laser diode to create an interference pattern (hologram) that is reconstructed by software into images. HoloStudio software (Phase Holographic Imaging AB)

was used for cellular segmentation, calculating quantitative features (optical thickness and volume), and individual cell tracking. Thirty-five cells were randomly chosen to quantitate the frequency of mitotic events. A cell volume greater than 2,500 μm^3 or a thickness greater than 8 μm was chosen as cutoff values for mitotic activity. To visualize the whole dynamic process, 4 dimensional (x-position, y-position, cell thickness coded as brightness over time) projections of the holograms were generated with the cell thickness threshold adjusted to show the mitotic cells (44, 45).

Immunofluorescence of β-tubulin

SKOV3-TR (2×10^4) cells were seeded onto coverslips placed in 6-well plates. After 24 hours, the cells were treated with liposomes (200 nmol/L paclitaxel) for 24 hours. After fixation, the cells were permeabilized with cold methanol, blocked with 3% BSA in PBS, and stained with the β-tubulin primary antibody (1:20) overnight at 4°C. The cells were then stained with FITC-labeled secondary antibodies (1:30) for 2 hours, 5 μmol/L of Hoechst 33342 for 30 minutes at room temperature, and imaged by laser scanning confocal microscopy (Zeiss).

In vivo studies

Paclitaxel-resistant ovarian cancer Hey8-MDR (1×10^6) cells were injected intraperitoneally into 5- to 6-week-old athymic female nude mice. Eight days later, the mice were randomized into 3 groups (5 mice/group) and injected intraperitoneally with LP(PCT), LP(XR,PCT) (1.5 mg/kg paclitaxel; ∼1 mg/kg XR) or PBS 3 times per week. The injection was repeated 5 times. Body weights were measured 4 times within 20 days. The mice were euthanized 2 days after the fifth treatment and the tumor weight and numbers were recorded. The animal studies were repeated twice. Tumors failed to form in 1 and 2 mice in the LP(XR,PCT) and LP(PCT) treatment groups, respectively; these mice were therefore excluded from the assessment. The tumors were fixed in formalin, paraffin-embedded, and sectioned for subsequent immunohistochemical and hematoxylin and eosin (H&E) staining. Immunohistochemical staining of human ovarian tumor sections was performed to assess markers of apoptosis (cleaved caspase-3, Asp175, 1:20) and proliferation (Ki67, SP6, 1:300). The slides (5 slides/group) were imaged at 200× magnification from three random fields (46); stained cells were quantified using NIH ImageJ software (28).

Statistical analysis

Data were expressed as means ± SEM. Statistical analyses were performed using two-tailed t test or ANOVA (47, 48) with GraphPad Prism. Significance was determined by $P < 0.05$ (*), $P < 0.01$ (**), and $P < 0.001$ (***).

Results

P-gp overexpression is associated with poor prognosis in patients with ovarian cancer

Several reports have indicated that P-gp plays an important biologic and prognostic role in the acquisition of MDR in a wide range of human cancers, including ovarian cancer. However, the number of patients in these studies was small (19–22). We, therefore, interrogated two publicly available datasets to determine whether *P-gp* mRNA expression is associated with the survival of ovarian cancer patients (Fig. 1,

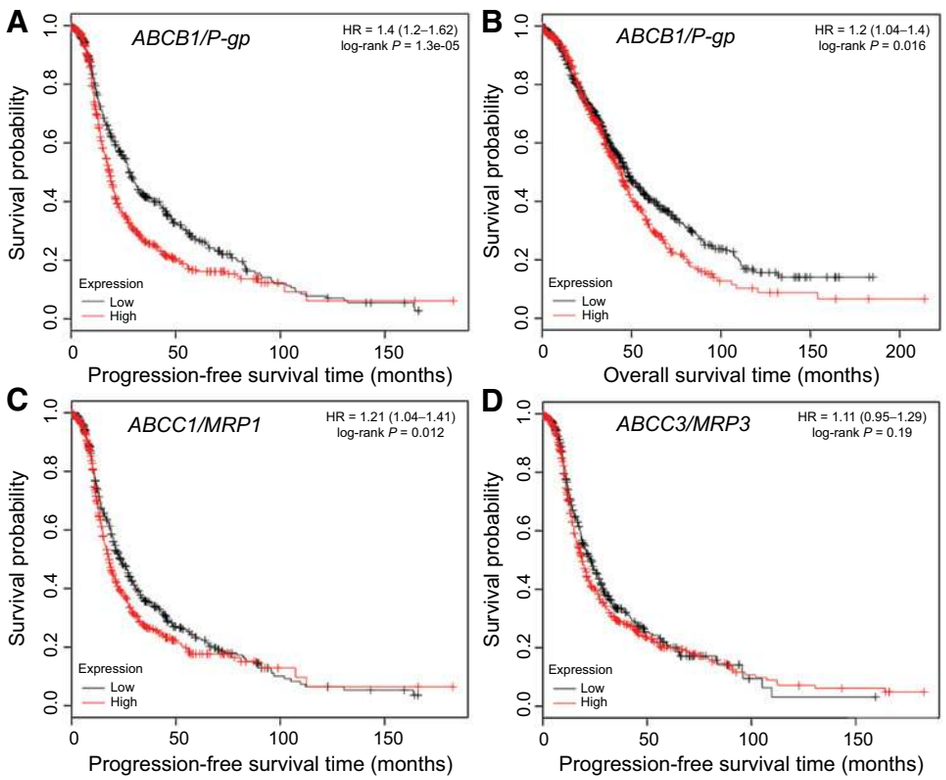

Figure 1.
Correlation between P-gp expression and ovarian cancer patient survival using two datasets. The cut-off level of expression dividing the high or low groups was calculated by an algorithm of the Kaplan–Meier plotter. **A,** progression-free survival (PFS) analysis of *P-gp/ABCB1* gene ($n = 1{,}106$; log-rank: $P = 1.3 \times 10^{-5}$). The cut-off level was determined at 43 to divide high ($n = 420$) and low ($n = 686$) groups. **B,** overall survival (OS) analysis of *ABCB1* gene, which encodes for the P-gp protein ($n = 1{,}339$; log-rank: $P = 0.016$). The cut-off level was determined at 64 to divide high ($n = 520$) and low ($n = 819$) expression groups. **C,** PFS analysis of *MRP1/ABCC1* gene, which encodes for the MRP1 protein ($n = 1{,}056$; log-rank: $P = 0.012$). The cut-off level was determined at 393 to divide high ($n = 595$) and low ($n = 461$) expression groups. **D,** PFS analysis of *MRP3/ABCC3* gene ($n = 1{,}056$; log-rank: $P = 0.19$). The cut-off level was determined at 101 to divide high ($n = 653$) and low ($n = 403$) expression groups.

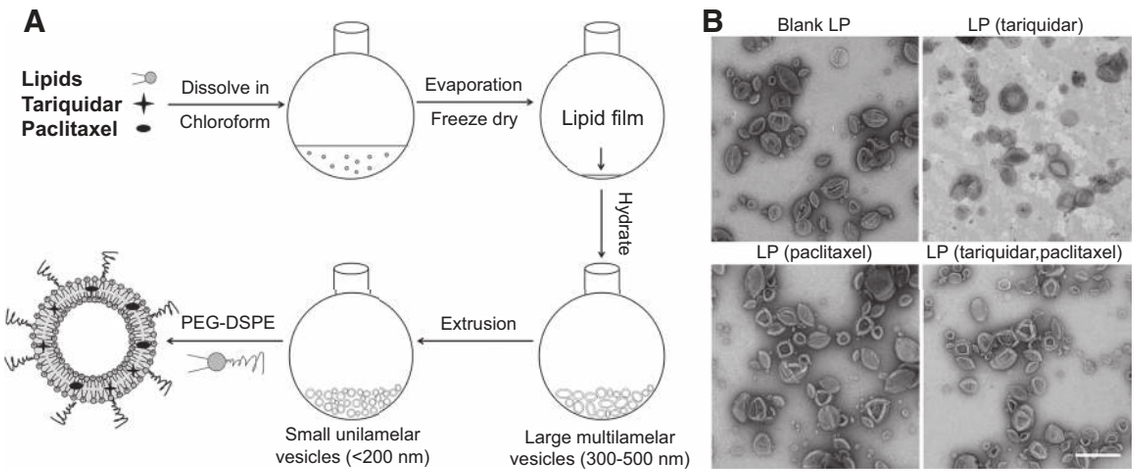

Figure 2.
Synthesis and characterization of drug-loaded liposomes. **A,** schematic of liposome preparation. **B,** transmission electron micrographs of liposomes (LP) encapsulated with no drugs (blank), tariquidar (XR), or paclitaxel (PCT), using a negative staining technique with uranyl acetate. Scale bar, 500 nm.

TCGA, GEO datasets; refs. 7, 37). Kaplan–Meier analysis of more than 1,000 patients showed that high expression of *P-gp* is significantly correlated with shorter PFS ($n = 1{,}106$; log-rank: $P = 1.3 \times 10^{-5}$, HR = 1.4, Fig. 1A) and OS ($n = 1{,}339$; log-rank: $P = 0.016$, HR = 1.2, Fig. 1B). Expression of *MRP1*, which confers resistance to vinca alkaloids, but not to taxanes, was associated with reduced PFS ($P = 0.012$, HR = 1.21, Fig. 1C), but not with OS (data not shown). In contrast, the expression of *MRP3* (*ABCC3*), another ABC transporter, was not correlated with PFS ($P = 0.19$, HR = 1.11, Fig. 1D). This is consistent with results from a previous study that analyzed the correlation of the expression of P-gp, MRP1, and MRP3 with PFS using immunohistochemical staining in 111 patients with ovarian cancer (19).

Preparation and characterization of liposomes loaded with tariquidar and paclitaxel

In view of the strong prognostic value of P-gp in ovarian cancer (Fig. 1) and the encouraging preclinical results obtained by blocking P-gp with shRNA (23), we worked on improving specific tumor delivery of the third-generation P-gp inhibitor tariquidar using liposomes (35). These drug carriers have favorable pharmacokinetic profiles and minimal side effects. The well-defined nanoparticles were prepared through a multistep procedure (35). Liposomes were assembled from ePC, cholesterol, and DOTAP, with the drugs tariquidar and paclitaxel. Then using the postinsertion technique, PEG_{2000}-DSPE was inserted into the liposomes (Fig. 2A). Transmission electron microscopy images showed that the nanoparticles were spherical or elliptical in shape with a smooth surface (Fig. 2B). DOTAP was used to make the liposomes cationic, facilitating cellular uptake, endosomal escape, and subsequent drug release. PEG coating and the cationic charge of the liposomes increased their stability in solution and increased their circulating half-life. After careful optimization of this process, the resulting liposomes demonstrated favorable physicochemical properties, as evidenced by size, polydispersity index, and zeta potential (Supplementary Table S1).

LP(XR,PCT) inhibited the cell growth and proliferation of chemoresistant ovarian cancer cells *in vitro*

Using 3 well-characterized chemosensitive/chemoresistant ovarian cancer cell line pairs, we evaluated the expression of P-gp and MRP1 by flow cytometry (Fig. 3A). While there was no significant difference in MRP1 expression between the chemosensitive and chemoresistant cell lines in all 3 cell line pairs, P-gp expression was significantly higher in the paclitaxel-resistant cell lines HeyA8-MDR (2.4-fold) and SKOV3-TR (1.9-fold) than in their sensitive parental counterparts. No significant difference in P-gp expression was observed between the carboplatin-resistant Tyn-Nu-R cell line and its parental carboplatin-sensitive Tyk-Nu cell line (33). The elevated expression of P-gp in HeyA8-MDR and SKOV3-TR cells, compared with HeyA8 and SKOV3ip1, respectively, was confirmed by immunoblot analysis (Fig. 3B). Flow cytometric analysis of fluorescent rhodamine 123 efflux revealed that chemosensitive cells had greater retention (~20-fold) of rhodamine 123 than chemoresistant cells (Fig. 3C). However, tariquidar efficiently blocked the efflux of rhodamine 123 from the paclitaxel-resistant, P-gp overexpressing HeyA8-MDR and SKOV3-TR cells. This effect was even more pronounced in experiments using the liposomal tariquidar; importantly, these liposomes only contained approximately 10% of the free tariquidar concentration, implying that the cellular uptake of tariquidar is enhanced in the liposomal formulation. In contrast, neither free nor liposomal tariquidar had a significant effect on the retention of rhodamine 123 in Tyn-Nu R cells (data not shown). These data suggest that tariquidar efficiently inhibits drug exclusion in chemoresistant ovarian cancer cells.

Next, the functional effects of the tariquidar/paclitaxel-loaded liposomes [LP(XR,PCT)] in the chemosensitive/chemoresistant ovarian cancer cell line pairs were investigated. The results from MTT cytotoxicity (Supplementary Methods and Supplementary Fig. S1A and S1B) and fluorescence-based viability (Fig. 4A) assays showed that both the paclitaxel-only liposomes [LP(PCT)] and the paclitaxel/tariquidar liposomes affected cell viability in the sensitive cell lines. In the chemoresistant cells, paclitaxel alone had a more limited effect;

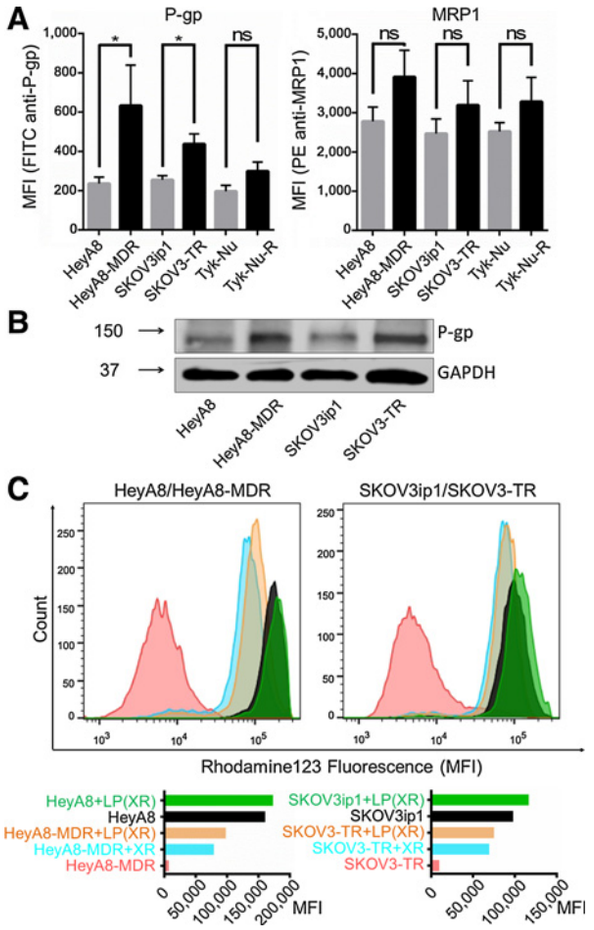

Figure 3.

Tariquidar inhibits P-gp activity in chemoresistant ovarian cancer cells. **A,** flow cytometric analysis of P-gp and MRP-1 expression. Three pairs of chemotherapy-sensitive (HeyA8, SKOV3ip1, Tyk-Nu) and -resistant (HeyA8-MDR, SKOV3ip1-TR, Tyk-Nu-R) ovarian cancer cell lines were stained with either FITC-labeled anti–P-gp or PE-labeled anti-MRP1 antibody. **B,** immunoblot analysis of P-gp expression in HeyA8, HeyA8-MDR, SKOV3ip1, and SKOV3-TR cells. **C,** rhodamine123 exclusion assay to measure efflux. The sensitive and resistant cell line pairs, HeyA8/HeyA8-MDR and SKOV3ip1/SKOV3-TR cells, were treated with free tariquidar (140 nmol/L XR) or liposomal XR (14 nmol/L XR) for 2 days, stained with rhodamine 123, and analyzed by flow cytometry. MFI, mean fluorescence intensity. Columns represent means ± SEM from three independent experiments. *, $P < 0.05$; ns, not significant, two-tailed *t*-test.

the IC_{50} of LP(PCT) was in the micromolar (1–2 μmol/L) range; however, the IC_{50} of LP(XR,PCT) in these cells was in the nanomolar (2–10 nmol/L) range (Supplementary Fig. S1A and S1B). Similar results were obtained using a second, fluorescence-based cell viability assay, confirming that the dual drug-loaded liposomes could efficiently decrease cell viability by 87% and 95% in HeyA8-MDR and SKOV3-TR cells, respectively (Fig. 4A).

Paclitaxel blocks mitotic spindle assembly by binding to microtubules, thereby inhibiting cell division, migration, and proliferation (42, 49). Therefore, these effects were measured to determine whether LP(XR,PCT) could resensitize paclitaxel-resistant ovarian cancer cells to paclitaxel treatment. In the sensitive cells, both LP(PCT) and LP(XR,PCT) induced a G_2–M arrest (58.9% vs. 59.3%), but in the resistant cells, only LP(XR,PCT) induced and maintained a significant G_2–M arrest (65.5% vs. 32.1%; Fig. 4B and Supplementary Fig. S1C). The observation was further confirmed by laser scanning cytometry (50) and immunoblot analysis (Fig. 4B, bottom). LP(XR,PCT) treatment decreased the percentage of DNA in G_1 and increased the percentage of DNA in G_2 (laser scanning cytometry, data not shown). It also decreased CDC25C and phosphorylated CDC2 protein expression and increased cyclin B1 levels (Fig. 4B, bottom). Next, the LP(XR,PCT) effect on migration was determined using the IncuCyte live-cell imaging system (Fig. 4C, Supplementary Fig. S1D). In chemosensitive HeyA8 cells, both LP(PCT) and LP(XR,PCT) inhibited cell motility by 58.8% and 66.8%, respectively. In the paclitaxel-resistant cells only LP(XR,PCT) was effective, resulting in the almost complete inhibition of cell migration.

Next, the effect of LP(XR,PCT) on cell proliferation was examined; to this end, both a monolayer and a 3D soft agar colony formation assay were utilized (Fig. 4D). The dual drug-loaded liposomes completely blocked colony formation in the paclitaxel-resistant SKOV3-TR cells. The effect of the liposome preparations on the adhesion and invasion of ovarian cancer cells was tested using an organotypic 3D culture model (51) in which ovarian cancer cells were cocultured with human primary stromal cells. Liposome preparation affected the neither adhesion nor invasion of ovarian cancer cells (Supplementary Methods and Supplementary Fig. S2). In summary, the data demonstrated that in 2 chemoresistant ovarian cancer cell clones, LP(XR,PCT) increased cytotoxicity, inhibited cell mitosis, migration, colony formation, and proliferation but did not affect adhesion or invasion.

LP(XR,PCT)-mediated apoptosis follows mitotic arrest due to paclitaxel-induced tubulin polymerization

The microtubule-stabilizing activity of paclitaxel causes G_2–M arrest and mitotic catastrophe, followed by apoptosis (42, 49). Three imaging techniques were used to characterize the effects of LP(XR,PCT) on tubulin polymerization (Fig. 5A), mitotic arrest (Fig. 5B), and apoptosis (Fig. 5C) in SKOV3-TR cells. Immunofluorescent analysis of β-tubulin expression showed that both untreated and LP(PCT)-treated cells were flat, with fibrils extending from the nucleus to the cell periphery (Fig. 5A). However, treatment with LP(XR,PCT) led to cell rounding and ring-like β-tubulin formations around the nucleus; this was consistent with the treatment of paclitaxel-sensitive cells (data not shown) and previous reports (49).

Label-free holographic imaging cytometry is a form of time lapse microscopy that allows noninvasive monitoring and quantification of cell behavior, such as mitosis and mitotic arrest (52). Treatment of paclitaxel-resistant SKOV3-TR cells with LP(XR,PCT) induced mitotic arrest, as evidenced by increased cellular thickness (red) and larger cell volume (Fig. 5B, left). Several cells were unable to complete cell division 24 hours after onset of mitosis (Supplementary Videos S1–S3 and Supplementary Fig. S3). To better assess dynamic cell changes, we generated 4D projections of 3 spatial dimensions (*x*, *y*, and local cell thickness) over time and quantified the frequency of mitotic arrest, defined as cells with an average volume > 2,500 μm^3. In the untreated and LP(PCT) groups, small "V-shaped" spots were observed, representing the effective completion of mitosis (parent cell to 2 daughter cells). "Short streaks", representing "delayed" mitotic events, were occasionally observed in the

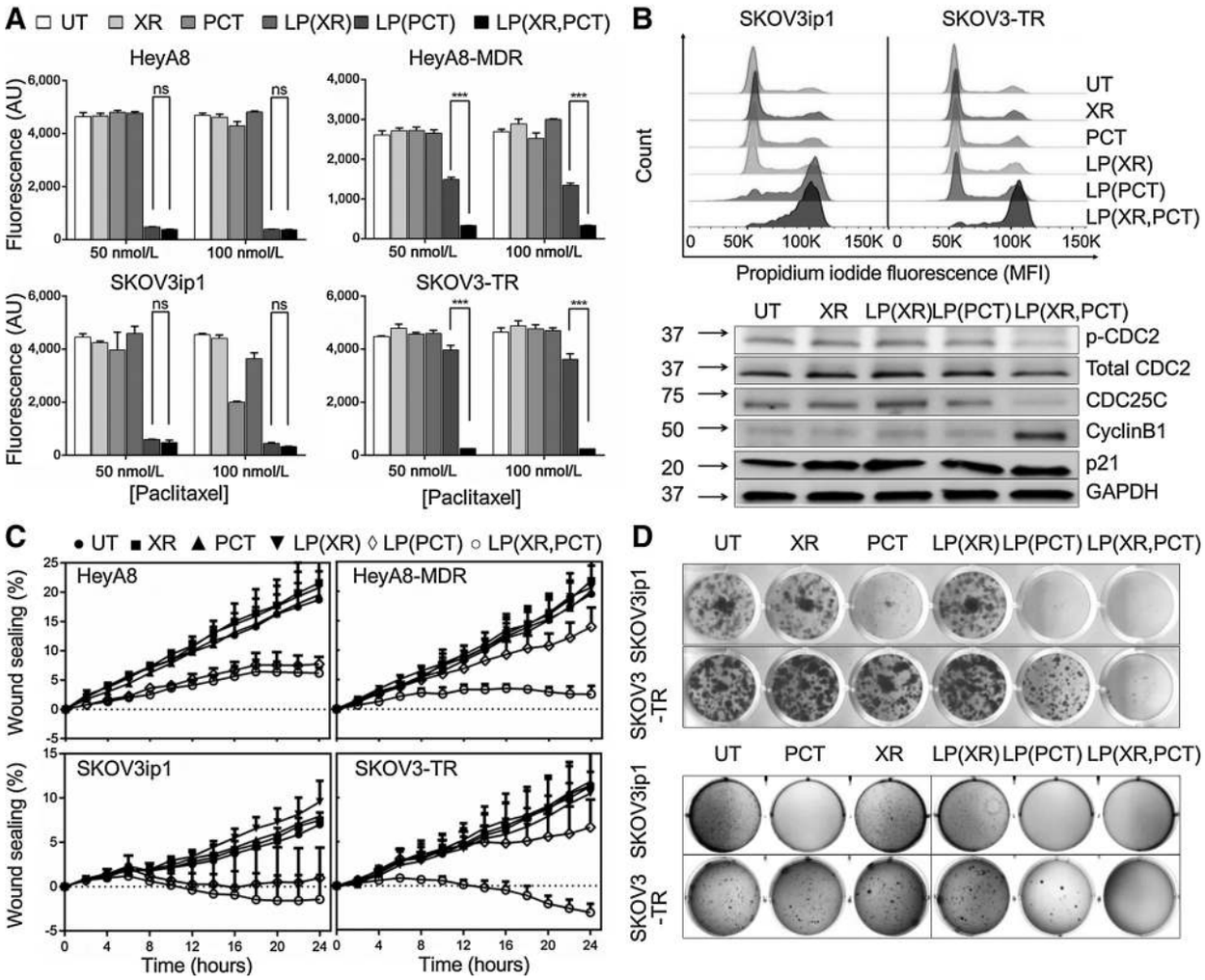

Figure 4.

Liposomal tariquidar/paclitaxel blocks proliferation, migration, and colony formation of chemoresistant ovarian cancer cells. The chemosensitive (HeyA8, SKOV3iP1) and chemoresistant cell lines (HeyA8-MDR, SKOV3-TR) were seeded and treated with tariquidar (XR), paclitaxel (PCT), liposomal (LP) XR [LP(XR)], LP(PCT), LP(XR,PCT), or left untreated (UT). **A,** cell viability. Cells were treated with paclitaxel for 7 days and viability measured. **B,** cell-cycle analysis. Top, cells were treated with paclitaxel (100 nmol/L) or tariquidar (90 nmol/L) for 18 hours before fixation, PI staining, and flow cytometric analysis. Bottom, immunoblot analysis of phosphorylated (Y15) CDC2, total CDC2, CDC25C, cyclin B1, and p21 in HeyA8-MDR cells upon liposome treatments (PCT, 100 nmol/L; XR, 90 nmol/L; 18 hours). **C,** cell migration. Cells were scratched, treated with drugs (50 nmol/L PCT; 45 nmol/L XR) and imaged every 2 hours for 24 hours using the IncuCyte Live Cell Imaging System. Wound confluence was determined using Zoom software. Columns represent means ± SEM from two independent experiments. **D,** colony formation. Top, monolayer colony formation. Cells were treated (100 nmol/L PCT; 90 nmol/L XR) for 7 days before fixation, crystal violet staining, and imaging. Bottom, soft agar colony formation. Cells were treated with the indicated drugs at the same concentrations for 40 days before fixation, crystal violet staining, and imaging. ***, $P < 0.001$; ns, not significant, two-tailed t test.

untreated group; in these cases, the cells sometimes took a few hours longer to complete mitosis, which could reflect the dependence, suggested by previous studies (53), of Taxol-resistant cells on paclitaxel to complete mitosis. This dependence may account for the 8.8% mitotic arrest rate observed in the untreated group as opposed to 0% in the LP(PCT) group. "Longer streaks" were predominantly observed in the LP(XR, PCT) group, indicating that the 82.7% of all imaged cells underwent mitotic arrest; they progressively increased in volume and thickness over a long period of time until cell death (Supplementary Videos S1–S3). In addition, the cells displayed a wave-shaped pattern of volume changes, representative of the division of the parental cells (large volume) into daughter cells (small volume; Fig. 5B, right).

The apoptosis-inducing potential of the liposomes was evaluated using fluorescent dyes semispecific for early/late apoptosis and detected with laser scanning cytometry (ref. 50; Fig. 5C). Compared with LP(PCT), LP(XR,PCT) induced massive apoptosis/necrosis (39.9% vs. 3.1%, $P < 0.001$) and the emergence of apoptotic bodies (Fig. 5C, inset), indicative of late apoptosis (54). When SKOV3-TR cells were treated with several different paclitaxel concentrations, the dual-agent liposomes always achieved the strongest induction of late apoptosis/necrosis (Supplementary Fig. S4).

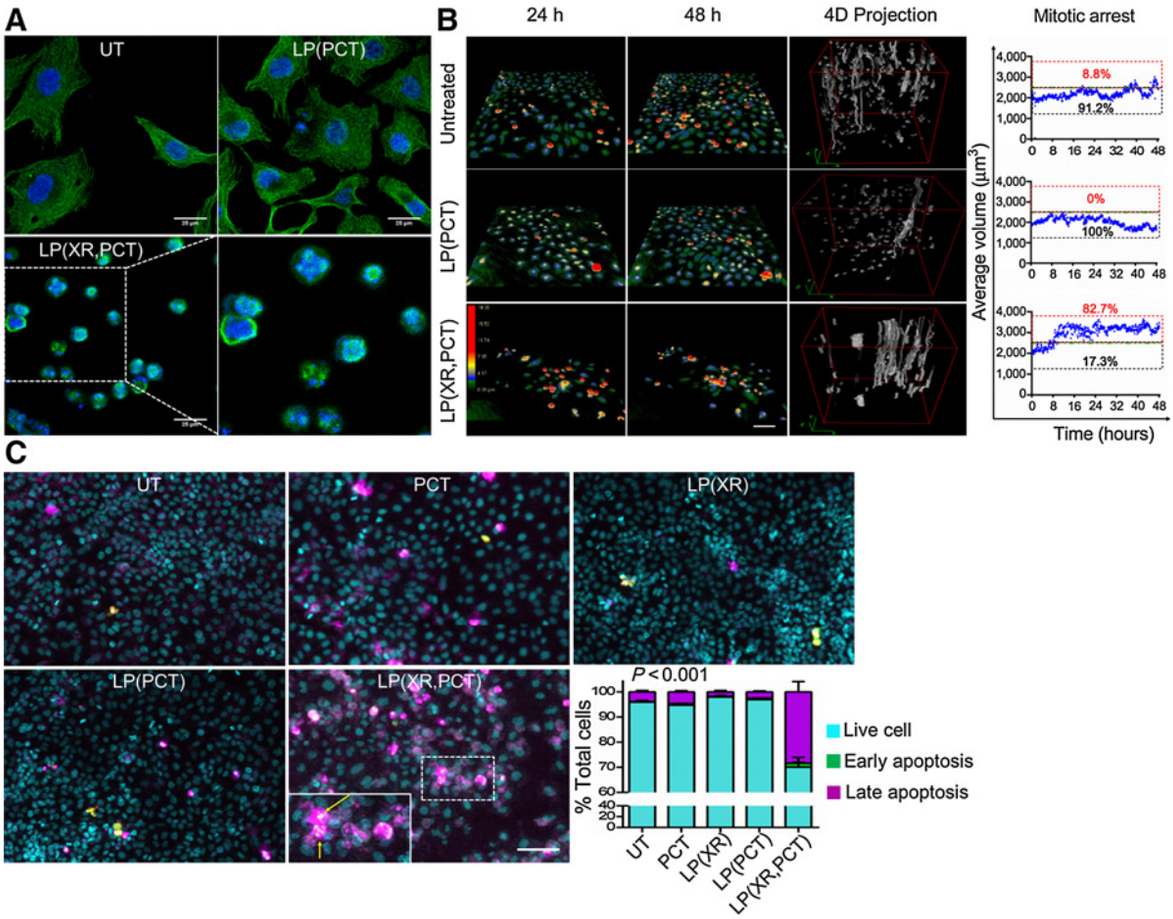

Figure 5.

Liposomal tariquidar/paclitaxel–mediated apoptosis following mitotic arrest due to paclitaxel-induced tubulin polymerization. **A,** confocal microscopy. Immunofluorescent detection of β-tubulin. Images show paclitaxel-induced β-tubulin dysfunction in paclitaxel-resistant SKOV3-TR cells treated with liposomal tariquidar/paclitaxel [LP(XR,PCT)]. Blue, Hoechst; green, β-tubulin. Scale bar, 25 μm. **B,** holographic imaging cytometry. SKOV3-TR cells were treated with either LP(PCT) or LP(XR,PCT) and visualized by HoloMonitor M4 every 5 minutes for 48 hours. 3D representation of holographic images of cells at 24- or 48-hour treatment is shown. Pseudocoloring of cells allows gauging of cell thickness. Green depicts cells with low optical thickness, such as flat interphase cells, whereas red indicates cells with high thickness such as rounded cells in mitosis. Middle, 4D projection. "Longer streaks" as seen in the LP(XR,PCT) group show mitotic arrest, as these cells are unable to divide and progressively increase in volume and thickness over a long period of time until cell death. Scale bar, 25 μm. Right, quantification of mitotic arrest with data shown in the left (2,500 μm^3, a threshold for average volume). **C,** laser scanning cytometry to detect apoptosis. SKOV3-TR cells were treated (150 nmol/L, PCT) for 24 hours and recovered for 24 hours. The cells were stained with Hoechst (cyan, nuclei), Yo-Pro (green, early apoptosis), and PI (magenta, late apoptosis). Insert, apoptotic bodies are indicated by yellow arrows. Scale bar, 50 μm. In LP(XR,PCT), there are fewer cells because of the combination of reduced cell proliferation and induced apoptosis. Two-way ANOVA.

Dual paclitaxel/tariquidar-loaded liposomes inhibit cell growth and metastasis

To evaluate the effect of the combined liposomes *in vivo*, we used the same ovarian cancer cell lines in an orthotopic ovarian cancer xenograft model (Fig. 6). HeyA8-MDR cells were intraperitoneally inoculated into female athymic nude mice, and 8 days later, mice were randomized into three groups (paclitaxel/tariquidar liposomes vs. paclitaxel liposomes vs. control) and intraperitoneally injected with liposomes 3 times per week with a total of five treatments (Fig. 6A). Analysis of two independent xenograft experiments showed that all treatment groups had minimal toxicity and similar gains in body weight (Fig. 6B). In the HeyA8-MDR tumor–bearing mice, which only produced a few solid tumors, treatment with the dual liposomes resulted in a significant reduction in mean tumor weight (43.2% vs. 16.9%, $P = 0.0007$) and number of metastases (44.4% vs. 2.8%, $P = 0.012$), compared with LP(PCT)-treated mice (Fig. 6C and D).

To study the effects of tariquidar alone, free and liposomal XR was tested using again the orthotopic ovarian cancer xenograft model and regimen shown in Fig. 6A. The results showed neither free nor liposomal XR significantly affected tumor weight, number of metastases, or body weight compared with PBS-treated mice (Supplementary Methods and Supplementary Fig. S5A). In surrogate studies, LP(XR) showed a potent (3-fold) and durable (2 days post fifth injection) inhibition of Rhodamine 123 efflux in HeyA8-MDR tumors *ex vivo*, suggesting the efficient delivery and accumulation of LP(XR) in the tumors (Supplementary Methods and Supplementary Fig. S5B).

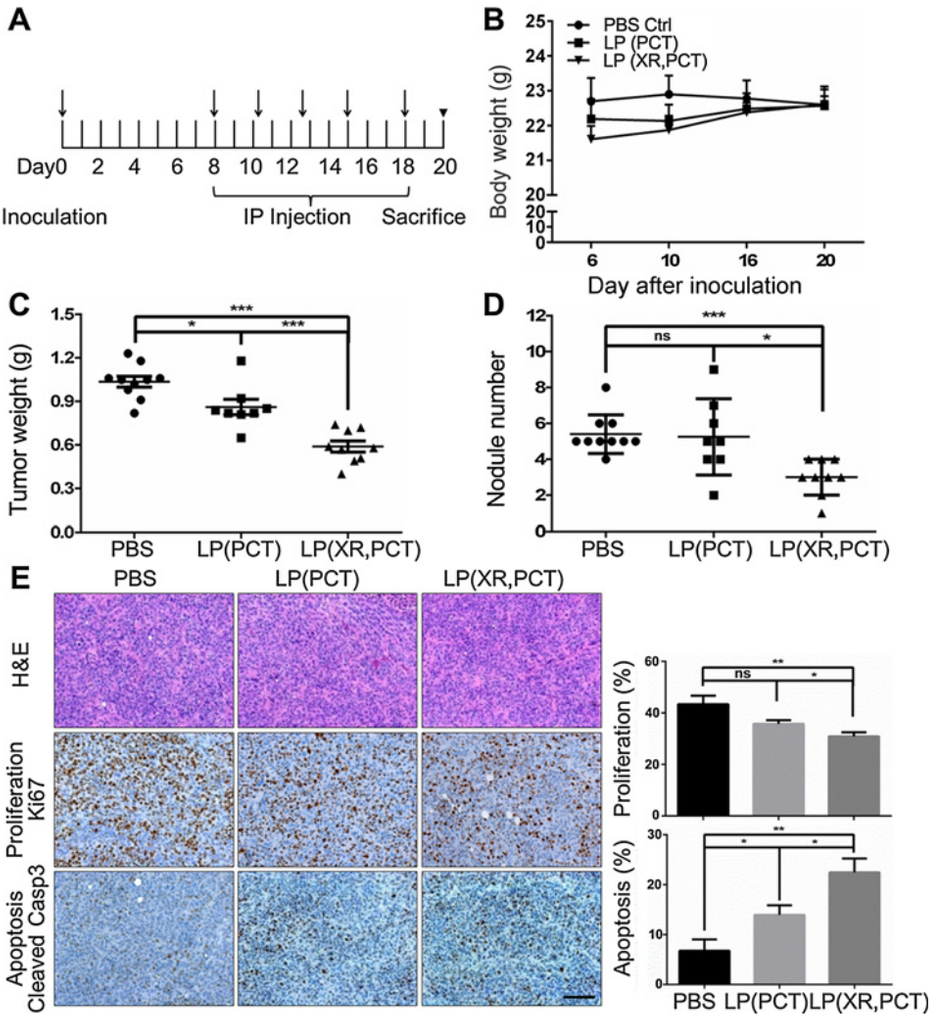

Figure 6.

Paclitaxel and tariquidar-loaded liposomes reduced tumor burden in a chemoresistant ovarian cancer xenograft mouse model. **A,** timeline. One million paclitaxel-resistant HeyA8-MDR cells were intraperitoneally (IP) inoculated into female athymic nude mice (arrow). Eight days later, 15 mice were randomized into 3 groups ($n = 5$ mice) and treated IP with either liposomal paclitaxel [LP(PCT)] (■), liposomal tariquidar/paclitaxel [LP(XR,PCT)] (▲) (1.5 mg/kg, PCT; ∼1 mg/kg, XR) or PBS (●). **B,** body weight. **C,** tumor weight. **D,** metastasis. Columns represent means ± SEM from two independent experiments ($n > 8$ mice). Two and one mouse failed to form tumor in LP(PCT) and LP(XR, PCT) groups, respectively, and therefore were excluded from the assessment. **E,** H&E staining and immunohistochemistry for cleaved caspase-3 (apoptosis) and Ki-67 (proliferation). Scale bar, 100 μm. The percentage of Ki-67–positive cells and cleaved caspase-3–positive cells over total cells was quantified by ImageJ (right). Bars, means ± SEM ($n = 5$ mice). ***, $P < 0.001$; **, $P < 0.01$; *, $P < 0.05$. ns, not significant, two-tailed t test.

To explore the mechanism underlying the reduction in tumor burden in HeyA8-MDR tumor–bearing mice treated with dual liposomes, we performed H&E and immunohistochemical staining for molecular markers of apoptosis (cleaved caspase-3), proliferation (Ki-67), microvessel density (CD31), and macrophage infiltration (F4/80; Fig. 6E, Supplementary Materials and Methods and Supplementary Fig. S5C). H&E staining consistently showed that HeyA8-MDR tumors were high-grade and undifferentiated. The LP(XR,PCT) had no effect on angiogenesis and macrophage infiltration (Supplementary Fig. S5C). However, consistent with our *in vitro* results, the dual drug-loaded liposome-treated tumors showed impaired proliferation and a higher rate of apoptosis (Fig. 6E).

Discussion

Paclitaxel, alongside carboplatin, is one of the two most commonly used antimitotic drugs for ovarian cancer chemotherapy in the adjuvant setting and, for patients with platinum-sensitive ovarian cancer, in the recurrent setting (55). A previous study correlating the expression of various drug transporters with chemoresistance to 119 drugs reported that paclitaxel resistance had the fourth highest correlation with P-gp expression in the NCI-60 cell line panel (9). Several reports (19–22), including this one, show that high expression of P-gp is consistently associated with a poor clinical outcome in patients with ovarian cancer; although this association has not been observed by all (56). In several clinical trials (4, 26), tariquidar, a third-generation P-gp inhibitor, has demonstrated a good safety profile and has been shown to induce potent blockage of P-gp efflux activity, enabling paclitaxel to get into cells (10). Yet, the efficient reversal of drug resistance by coadministration of the P-gp inhibitor and anticancer drugs has not been achieved, largely because of the lack of a systemic delivery platform that can specifically supply effective levels of the drugs to malignant tissue (10).

We previously synthesized a liposome coloaded with tariquidar and paclitaxel and demonstrated that the liposomes reversed resistance to paclitaxel *in vitro*. However, the mechanism of action remained unclear and no *in vivo* data were provided (35). We extend Patel and colleagues' findings to show that, when paired with tariquidar, paclitaxel is able to block the proliferation, migration, and colony formation of chemoresistant ovarian cancer cells as effectively, as it blocks these functions in the

chemosensitive parental cells. To facilitate the assessment of therapeutic efficacy of this formulation in animal studies, we successfully increased the loading amounts of both tariquidar and paclitaxel by approximate 20-fold without affecting physicochemical features of the liposomes. Experiments using the liposomes with preclinical mouse models confirmed these results *in vivo*, showing that tariquidar resensitizes chemoresistant ovarian cancer cells to paclitaxel treatment, allowing paclitaxel to induce apoptosis in established tumors. This is consistent with previous *in vitro* results using the P-gp substrate doxorubicin. The IC_{50} for doxorubicin was much lower in the presence of tariquidar and inhibition of cell growth persisted, despite removal of tariquidar from the media (57).

The dual encapsulation of tariquidar and paclitaxel into nanoparticles ensures that they will be internalized by ovarian cancer cells simultaneously and that the upload of both agents will involve the same pharmacokinetic profiles. To evaluate the mechanism of action of tariquidar in the liposome formulation, we employed advanced microscopic live-cell imaging approaches, such as kinetic cell monitoring (IncuCyte), laser scanning cytometry (iCyte), and holographic imaging cytometry (HoloMonitor M4). Because of its intrinsic ability to directly quantify phase shift and optical path length, holographic imaging circumvents optical artifacts, such as the shading-off effects and spurious asymmetry associated with the most widely used contrast-generating techniques (e.g., phase contrast and differential interference contrast) in optical microscopy (58). This label-free quantitative technique allowed us to follow the development of mitotic arrest in real-time. It permitted us to conclude that tariquidar treatment of paclitaxel-resistant cells resensitized the cells to paclitaxel, allowing the drug to induce almost complete mitotic arrest.

We also note that ovarian cancer may be particularly suitable for nanoparticle-facilitated MDR studies and treatment, because as many as 80% of epithelial ovarian tumors develop MDR. The dual drug-loaded liposomes increased the specific delivery of drugs to tumor cells and allowed tariquidar to become significantly more efficient in enabling paclitaxel to inhibit proliferation and colony formation, and promote cell-cycle arrest. The fact that the liposome platform significantly reduced tumor burden and metastasis in our mouse model suggests that we have identified an efficient vehicle for the delivery of paclitaxel and tariquidar specifically to the tumor for the reversal of MDR in chemoresistant ovarian cancer. Dual drug-loaded nanoparticles may be the next step toward bringing a P-gp inhibitor to the clinic.

Although MDR is especially common in ovarian cancer, appropriate patient selection is important if LP(XR,PCT) is to succeed as a therapeutic in chemoresistant ovarian cancer. In a recent study using whole-genome characterization of chemoresistant ovarian cancer (20), we reported a fusion protein, in which P-gp expression was driven by the promoter and exon 1 of SLC25A40 (a mitochondrial carrier protein) resulting in a fused transcript. This protein was detected in 8% of all recurrent, chemoresistant tumors that had been treated with paclitaxel, but not in chemosensitive tumors. Because paclitaxel can cause double strand breaks, it is probable that these genetic rearrangements were drug-induced (59). Given that clinical studies of P-gp inhibitors in unselected cases have had mixed results (60), selection of patients with P-gp overexpression or the SLC25A40/P-gp fusion protein may identify a patient subgroup that is more likely to respond to liposome-encapsulated tariquidar and paclitaxel.

Disclosure of Potential Conflicts of Interest

No potential conflicts of interest were disclosed.

Authors' Contributions

Conception and design: Y. Zhang, S.K. Sriraman, V. Torchilin, E. Lengyel
Development of methodology: Y. Zhang, S.K. Sriraman, E. Luther, V. Torchilin, E. Lengyel
Acquisition of data (provided animals, acquired and managed patients, provided facilities, etc.): Y. Zhang, S.K. Sriraman, E. Luther, V. Torchilin
Analysis and interpretation of data (e.g., statistical analysis, biostatistics, computational analysis): Y. Zhang, S.K. Sriraman, E. Luther, E. Lengyel
Writing, review, and/or revision of the manuscript: Y. Zhang, S.K. Sriraman, H.A. Kenny, V. Torchilin, E. Lengyel
Administrative, technical, or material support (i.e., reporting or organizing data, constructing databases): E. Lengyel
Study supervision: H.A. Kenny, V. Torchilin, E. Lengyel

Acknowledgments

We thank Gail Isenberg (University of Chicago), Dr. Karen Watters (University of Chicago), and Dr. Elena Holden (Executive Strategic Advisory) for editing this article. The authors also acknowledge the help of Dr. Marion Curtis in validating cell lines, Dr. Mark Eckert in survival analysis, and Jiayi Pan for liposome preparation. We thank the human tissue resource center and flow cytometry core facilities at the University of Chicago for their expert technical support. We would also like to thank William Fowle, Dr. Rajiv Kumar, and Dr. Srinivas Sridhar at Northeastern University for the physicochemical nanocharacterization.

Grant Support

This work was supported by NCI Alliance for Nanotechnology through a Cancer Nanotechnology Platform Partnership U01CA151461, a National Cancer Institute grant (NCI-R01 CA111882 to E. Lengyel) and by an NIH grant (U54CA151881 to V. Torchilin).

The costs of publication of this article were defrayed in part by the payment of page charges. This article must therefore be hereby marked *advertisement* in accordance with 18 U.S.C. Section 1734 solely to indicate this fact.

Received December 22, 2015; revised June 23, 2016; accepted July 13, 2016; published OnlineFirst July 27, 2016.

References

1. Siegel RL, Miller KD, Jemal A. Cancer statistics, 2015. CA Cancer J Clin 2015;65:5–29.
2. Lengyel E. Ovarian cancer development and metastasis. Am J Pathol 2010;177:1053–64.
3. Hartmann LC, Lu KH, Linette GP, Cliby WA, Kalli KR, Gershenson D, et al. Gene expression profiles predict early relapse in ovarian cancer after platinum-paclitaxel chemotherapy. Clin Cancer Res 2005;11: 2149–55.
4. Leonard GD, Fojo T, Bates SE. The role of ABC transporters in clinical practice. Oncologist 2003;8:411–24.
5. Armstrong DK, Bundy B, Wenzel L, Huang H, Baergen R, Lele S, et al. Intraperitoneal cisplatin and paclitaxel in ovarian cancer. N Engl J Med 2006;353:34–43.
6. Dano K. Active outward transport of daunomycin in resistant Ehrlich ascites tumor cells. Biochim Biophys Acta 1973;323:466–83.
7. Hedditch EL, Gao B, Russell AJ, Lu Y, Emmanuel C, Beesley J, et al. ABCA transporter gene expression and poor outcome in epithelial ovarian cancer. J Natl Cancer Inst 2014;106: pii: dju149.
8. Sharom FJ. ABC multidrug transporters: structure, function and role in chemoresistance. Pharmacogenomics 2008;9:105–27.

9. Huang Y, Anderle P, Bussey KJ, Barbacioru C, Shankavaram U, Dai Z, et al. Membrane transporters and channels: Role of the transportome in cancer chemosensitivity and chemoresistance. Cancer Res 2004;64:4294–301.
10. Szakacs G, Paterson JK, Ludwig JA, Booth-Genthe C, Gottesman MM. Targeting multidrug resistance in cancer. Nat Rev Drug Discov 2006;5: 219–34.
11. Su HY, Lai HC, Lin YW, Liu CY, Chen CK, Chou YC, et al. Epigenetic silencing of SFRP5 is related to malignant phenotype and chemoresistance of ovarian cancer through Wnt signaling pathway. Int J Cancer 2010; 127:555–67.
12. Rizzo S, Hersey JM, Mellor P, Dai W, Santos-Silva A, Liber D, et al. Ovarian cancer stem cell-like side populations are enriched following chemotherapy and overexpress EZH2. Mol Cancer Ther 2011;10:325–35.
13. Boyerinas B, Park SM, Murmann AE, Gwin K, Montag AG, Zillhardt M, et al. Let-7 modulates acquired resistance of ovarian cancer to taxanes via IMP-1 mediated stabilization of MDR1. Int J Cancer 2012;130:1787–97.
14. Frederick PJ, Green HN, Huang JS, Egger ME, Frieboes HB, Grizzle WE, et al. Chemoresistance in ovarian cancer linked to expression of microRNAs. Biotech Histochem 2013;88:403–9.
15. Loessner D, Stok KS, Lutolf MP, Hutmacher DW, Clements JA, Rizzi SC. Bioengineered 3D platform to explore cell-ECM interactions and drug resistance of epithelial ovarian cancer cells. Biomaterials 2010;31: 8494–506.
16. Thibault B, Castells M, Delord JP, Couderc B. Ovarian cancer microenvironment: implications for cancer dissemination and chemoresistance acquisition. Cancer Metastasis Rev 2014;33:17–39.
17. Juliano RL, Ling V. A surface glycoprotein modulating drug permeability in Chinese hamster ovary cell mutants. Biochim Biophys Acta 1976; 455:152–62.
18. Shen DW, Fojo A, Chin JE, Roninson IB, Richert N, Pastan I, et al. Human multidrug-resistant cell lines: increased mdr1 expression can precede gene amplification. Science 1986;232:643–5.
19. Sedlakova I, Laco J, Caltova K, Cervinka M, Tosner J, Rezac A, et al. Clinical significance of the resistance proteins LRP, Pgp, MRP1, MRP3, and MRP5 in epithelial ovarian cancer. Int J Gynecol Cancer 2015;25:236–43.
20. Patch AM, Christie EL, Etemadmoghadam D, Garsed DW, George J, Fereday S, et al. Whole-genome characterization of chemoresistant ovarian cancer. Nature 2015;521:489–94.
21. Penson RT, Oliva E, Skates SJ, Glyptis T, Fuller AFJr, Goodman A, et al. Expression of multidrug resistance-1 protein inversely correlates with paclitaxel response and survival in ovarian cancer patients: a study in serial samples. Gynecol Oncol 2004;93:98–106.
22. Zajchowski DA, Karlan BY, Shawver LK. Treatment-related protein biomarker expression differs between primary and recurrent ovarian carcinomas. Mol Cancer Ther 2012;11:492–502.
23. Duan Z, Brakora KA, Seiden MV. Inhibition of ABCB1 (MDR1) and ABCB4 (MDR3) expression by small interfering RNA and reversal of paclitaxel resistance in human ovarian cancer cells. Mol Cancer Ther 2004;3:833–8.
24. Roe M, Folkes A, Ashworth P, Brumwell J, Chima L, Hunjan S, et al. Reversal of P-glycoprotein mediated multidrug resistance by novel anthranilamide derivatives. Bioorg Med Chem Lett 1999;9:595–600.
25. Loo TW, Clarke DM. Tariquidar inhibits P-glycoprotein drug efflux but activates ATPase activity by blocking transition to an open conformation. Biochem Pharmacol 2014;92:558–66.
26. Fox E, Bates SE. Tariquidar (XR9576): a P-glycoprotein drug efflux pump inhibitor. Expert Rev Anticancer Ther 2007;7:447–59.
27. Kim BY, Rutka JT, Chan WC. Nanomedicine. N Engl J Med 2010;363: 2434–43.
28. Zhang Y, Kenny HA, Swindell EP, Mitra AK, Hankins PL, Ahn RW, et al. Urokinase plasminogen activator system targeted delivery of nanobins as a novel ovarian cancer therapeutics. Mol Cancer Ther 2013;12:2628–39.
29. Patil Y, Sadhukha T, Ma L, Panyam J. Nanoparticle-mediated simultaneous and targeted delivery of paclitaxel and tariquidar overcomes tumor drug resistance. J Control Release 2009;136:21–9.
30. Thaker PH, Yazici S, Nilsson M, Yokoi K, Tsan RZ, He J, et al. Antivascular therapy for orthotopic human ovarian carcinoma through blockade of the vascular endothelial growth factor and epidermal growth factor receptors. Clin Cancer Res 2005;11:4923–34.
31. Duan Z, Feller AJ, Penson RT, Chabner BA, Seiden MV. Discovery of differentially expressed genes associated with paclitaxel resistance using cDNA array technology: analysis of interleukin (IL) 6, IL-8, and monocyte chemotactic protein 1 in the paclitaxel-resistant phenotype. Clin Cancer Res 1999;5:3445–53.
32. Yoshiya N. [Establishment of a cell line from human ovarian cancer (undifferentiated carcinoma of FIGO classification) and analysis of its cell-biological characteristics and sensitivity to anticancer drugs]. Nihon Sanka Fujinka Gakkai Zasshi 1986;38:1747–53.
33. Yoshiya N, Adachi S, Misawa Y, Yuzawa H, Honda T, Kanazawa K, et al. [Isolation of cisplatin-resistant subline from human ovarian cancer cell line and analysis of its cell-biological characteristics]. Nihon Sanka Fujinka Gakkai Zasshi 1989;41:7–14.
34. Kenny HA, Lal-Nag M, White EA, Shen M, Chiang CY, Mitra AK, et al. Quantitative high throughput screening using a primary human three-dimensional organotypic culture predicts *in vivo* efficacy. Nat Commun 2015;6:6220.
35. Patel NR, Rathi A, Mongayt D, Torchilin VP. Reversal of multidrug resistance by co-delivery of tariquidar (XR9576) and paclitaxel using long-circulating liposomes. Int J Pharm 2011;416:296–9.
36. Matsuo Y, Park JH, Miyamoto T, Yamamoto S, Hisada S, Alachkar H, et al. TOPK inhibitor induces complete tumor regression in xenograft models of human cancer through inhibition of cytokinesis. Sci Transl Med 2014;6: 259ra145.
37. Gyorffy B, Lanczky A, Szallasi Z. Implementing an online tool for genome-wide validation of survival-associated biomarkers in ovarian-cancer using microarray data from 1287 patients. Endocr Relat Cancer 2012;19:197–208.
38. Lengyel E, Litchfield LM, Mitra AK, Nieman KM, Mukherjee A, Zhang Y, et al. Metformin inhibits ovarian cancer growth and increases sensitivity to paclitaxel in mouse models. Am J Obstet Gynecol 2014;212:479.e1–10.
39. Sriraman SK, Geraldo V, Luther E, Degterev A, Torchilin V. Cytotoxicity of PEGylated liposomes co-loaded with novel pro-apoptotic drug NCL-240 and the MEK inhibitor cobimetinib against colon carcinoma *invitro*. J Control Release 2015;220:160–8.
40. Bedner E, Li X, Gorczyca W, Melamed MR, Darzynkiewicz Z. Analysis of apoptosis by laser scanning cytometry. Cytometry 1999;35:181–95.
41. Mitra AK, Chiang CY, Tiwari P, Tomar S, Watters KM, Peter ME, et al. Microenvironment-induced downregulation of miR-193b drives ovarian cancer metastasis. Oncogene 2015;34:5923–32.
42. Ruttala HB, Ko YT. Liposomal co-delivery of curcumin and albumin/paclitaxel nanoparticle for enhanced synergistic antitumor efficacy. Colloids Surf B Biointerfaces 2015;128:419–26.
43. Liu Z, Yang X, Li Z, McMahon C, Sizer C, Barenboim-Stapleton L, et al. CASZ1, a candidate tumor-suppressor gene, suppresses neuroblastoma tumor growth through reprogramming gene expression. Cell Death Differ 2011;18:1174–83.
44. Minetti C, Podgorski T, Coupier G, Dubois F. Fully automated digital holographic processing for monitoring the dynamics of a vesicle suspension under shear flow. Biomed Opt Express 2014;5:1554–68.
45. Di Caprio G, El Mallahi A, Ferraro P, Dale R, Coppola G, Dale B, et al. 4D tracking of clinical seminal samples for quantitative characterization of motility parameters. Biomed Opt Express 2014;5:690–700.
46. Nieman KM, Kenny HA, Penicka CV, Ladanyi A, Buell-Gutbrod R, Zillhardt M, et al. Adipocytes promote ovarian cancer metastasis and provide energy for rapid tumor growth. Nat Med 2011;17:1498–503.
47. Alin A, Kurt S. Testing non-additivity (interaction) in two-way ANOVA tables with no replication. Stat Methods Med Res 2006;15:63–85.
48. Sasaki H, Sheng Y, Kotsuji F, Tsang BK. Down-regulation of X-linked inhibitor of apoptosis protein induces apoptosis in chemoresistant human ovarian cancer cells. Cancer Res 2000;60:5659–66.
49. Ahmed AA, Mills AD, Ibrahim AEK, Temple J, Blenkiron C, Vias M, et al. The extracellular matrix protein TGFBI induces microtubule stabilization and sensitizes ovarian cancers to paclitaxel. Cancer Cell 2007;12:514–27.
50. Darzynkiewicz Z, Smolewski P, Holden E, Luther E, Henriksen M, Francois M, et al. Laser scanning cytometry for automation of the micronucleus assay. Mutagenesis 2011;26:153–61.
51. Kenny HA, Chiang CY, White EA, Schryver EM, Habis M, Romero IL, et al. Mesothelial cells promote early ovarian cancer metastasis through fibronectin secretion. J Clin Invest 2014;124:4614–28.
52. Falck Miniotis M, Mukwaya A, Gjorloff Wingren A. Digital holographic microscopy for non-invasive monitoring of cell cycle arrest in L929 cells. PLoS One 2014;9:e106546.

53. Goncalves A, Braguer D, Kamath K, Martello L, Briand C, Horwitz S, et al. Resistance to Taxol in lung cancer cells associated with increased microtubule dynamics. Proc Natl Acad Sci U S A 2001;98: 11737–42.
54. Ashush H, Rozenszajn LA, Blass M, Barda-Saad M, Azimov D, Radnay J, et al. Apoptosis induction of human myeloid leukemic cells by ultrasound exposure. Cancer Res 2000;60:1014–20.
55. Fleming GF, Seidman JD, Lengyel E. Epithelial ovarian cancer. In:Barakat RR, Berchuck A, Markmann M, Randall ME, editors. Principles and practice of gynecologic oncology. Philadelphia, PA: Lippincott Williams & Wilkins; 2013. p.757–848.
56. Izquierdo MA, van der Zee AG, Vermorken JB, van der Valk P, Belien JA, Giaccone G, et al. Drug resistance-associated marker Lrp for prediction of response to chemotherapy and prognoses in advanced ovarian carcinoma. J Natl Cancer Inst 1995;87:1230–7.
57. Mistry P, Stewart AJ, Dangerfield W, Okiji S, Liddle C, Bootle D, et al. *In vitro* and *in vivo* reversal of P-glycoprotein-mediated multidrug resistance by a novel potent modulator, XR9576. Cancer Res 2001;61:749–58.
58. Marquet P, Depeursinge C, Magistretti PJ. Exploring neural cell dynamics with digital holographic microscopy. Annu Rev Biomed Eng 2013; 15:407–31.
59. Huff LM, Lee JS, Robey RW, Fojo T. Characterization of gene rearrangements leading to activation of MDR-1. J Biol Chem 2006;281:36501–9.
60. Abraham J, Edgerly M, Wilson R, Chen C, Rutt A, Bakke S, et al. A phase I study of the P-glycoprotein antagonist tariquidar in combination with vinorelbine. Clin Cancer Res 2009;15:3574–82.